Supporting information

Captions:

Fig. S1. The ^{1}H and ^{13}C NMR spectra of PAMs in CDCl$_3$.

Fig. S2.The spatial configurations of PAMs with the minimized energy at gas state. The dihedral angles of PAMs between the mean plane described by the central CZ and the C=N group which calculated by Density-functional theory.

Fig. S3. UV-vis spectra changes of PAM1, PAM2, PAM4 and PAM5 respectively, in the CH$_2$Cl$_2$ as they were protonated by HCl vapor in steps during the same time interval.

Fig. S4. UV–Vis absorption spectra change at 406 nm of PAM6 repeatedly placed in 1000 ppm HCl and NH$_3$ vapor.

Fig. S5. Cyclic voltammtry for ferrocene and 9-(2-ethylhexyl)-carbazole-3,6- dicarboxaldehyde in CH$_3$CN containing 0.1mol/L LiClO$_4$, at a scan rate of 50 mV/s.

Fig. S6. Cyclic voltammograms of PAM3 (A) and PAM5 (B) film on the ITO-coated glass substrate in at different scan rates: (a) 10, (b) 20, (c) 40, (d) 60, (e) 80, and (f)100 (e) 120 mV/s. Inset: Relationship of anodic and cathodic current peaks as a function of scan rate.

Fig. S7. The differential pulse voltammogram (DPV) of PAM2, PAM3 and PAM5 in CH$_3$CN containing 0.1mol/L LiClO$_4$, at a scan rate of 50 mV/s.

Fig. S8. CVs of PAM3 and PAM5 measured at scan rates between 10 and 120 mV/s. Inset: Randles–Sevcik plot of the oxidation (●) peaks of PAM3 and PAM5 relative to ferrocene (■) measured in dichloromethane with 0.5 M Bu$_4$ClO$_4$N as supporting electrolyte. Inset: Relationship of anodic current peaks as a function of the square root scan rate.

Fig. S9. Electronic absorption spectra of film of PAM1, PAM3, PAM4 and PAM6 membrane respectively, in the process of electrochemical doped with 0.1 V potential intervals in CH$_3$CN containing 0.1mol/L LiClO$_4$ as the supporting electrolyte (vs Ag/AgCl).
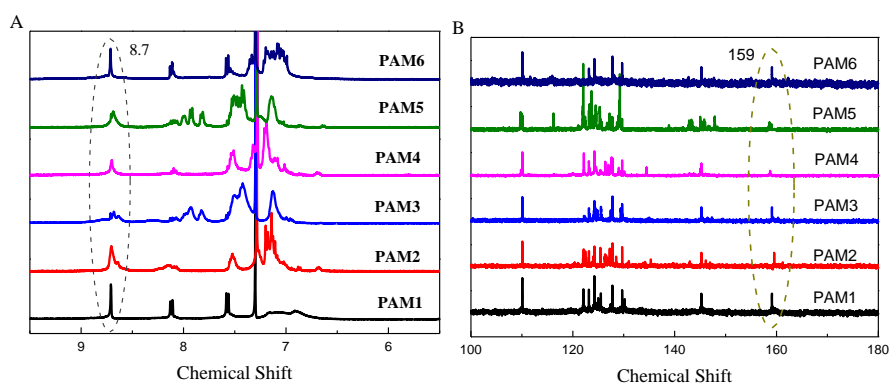
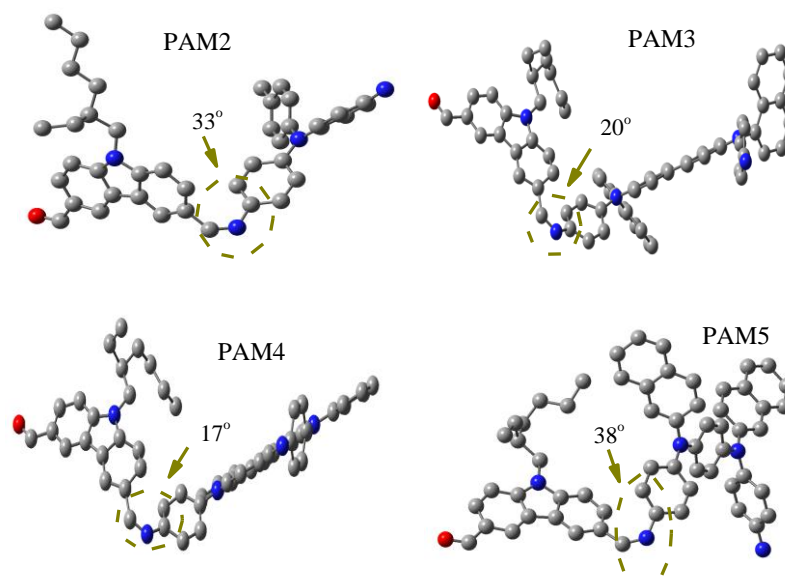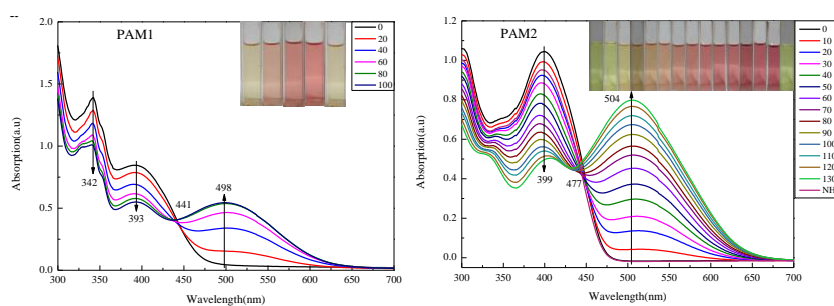Fig. S1. The ^{1}H and ^{13}C NMR spectra of PAMs in CDCl$_3$.

Fig. S2. The spatial configurations of PAMs with the minimized energy at gas state. The dihedral angles of PAMs between the mean plane described by the central CZ and the C=N group which calculated by Density-functional theory.
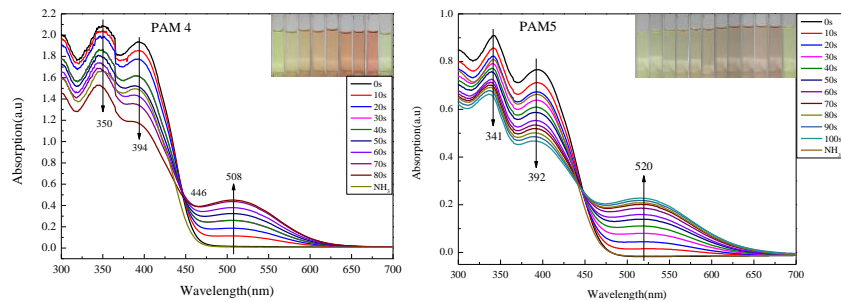
Fig. S3. UV-vis spectra changes of PAM1, PAM2, PAM4 and PAM5 respectively, in the CH$_2$Cl$_2$ as they were protonated by HCl vapor in steps during the same time interval.
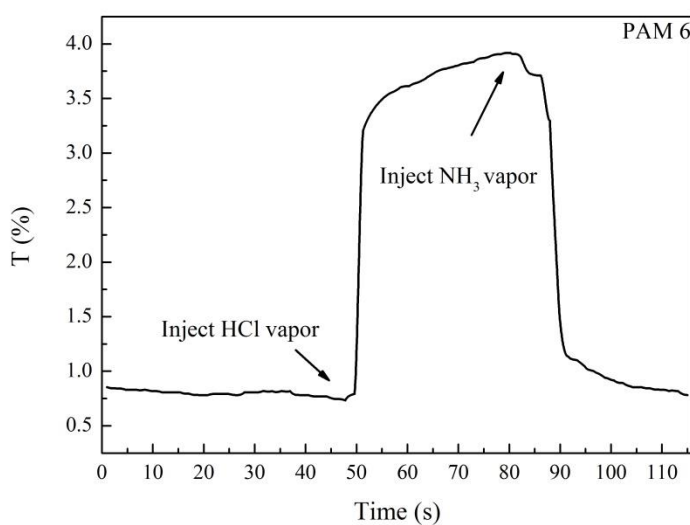

Fig. S4. UV–Vis absorption spectra change at 406 nm of PAM6 repeatedly placed in 1000 ppm HCl and NH$_3$ vapor.
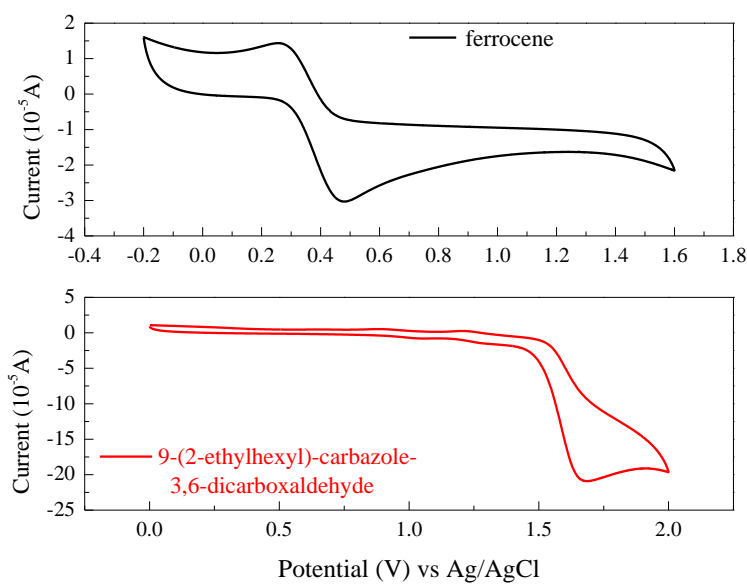
Fig. S5. Cyclic voltammetry for ferrocene and 9-(2-ethylhexyl)-carbazole-3, 6- dicarboxaldehyde in CH_3CN containing 0.1mol/L $LiClO_4$, at a scan rate of 50 mV/s.
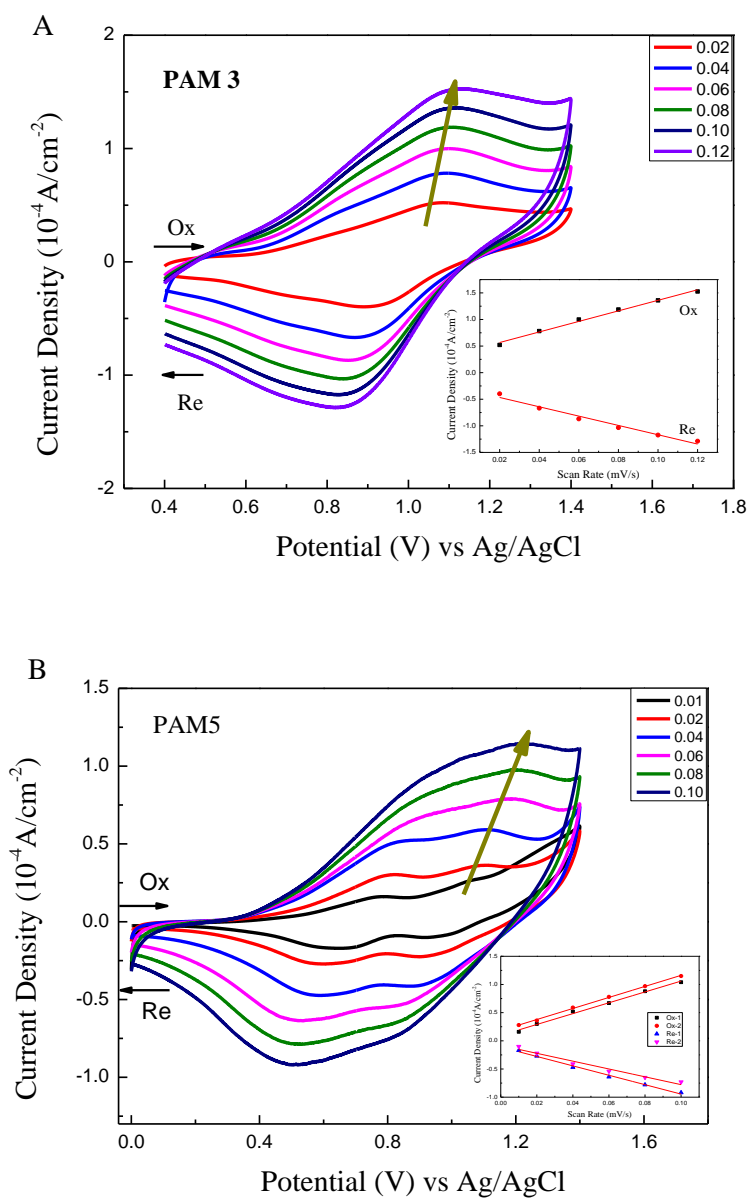

Fig. S6. Cyclic voltammograms of PAM3 (A) and PAM5 (B) film on the ITO-coated glass substrate in at different scan rates: (a) 10, (b) 20, (c) 40, (d) 60, (e) 80, and (f)100 (e) 120 mV/s. Inset: Relationship of anodic and cathodic current peaks as a function of scan rate.
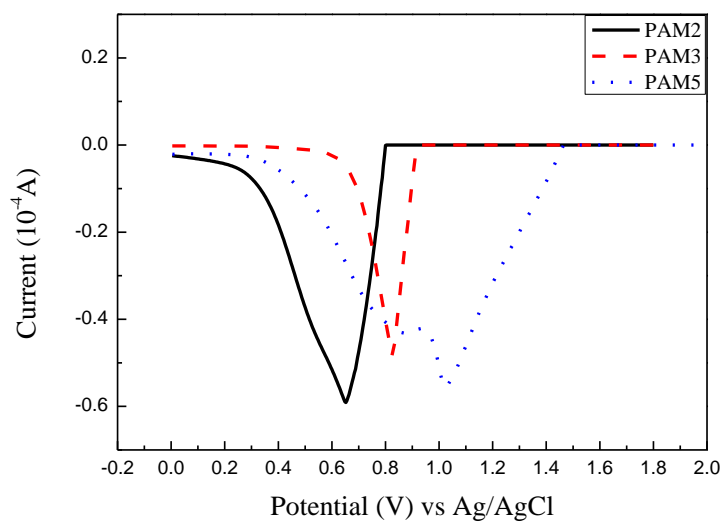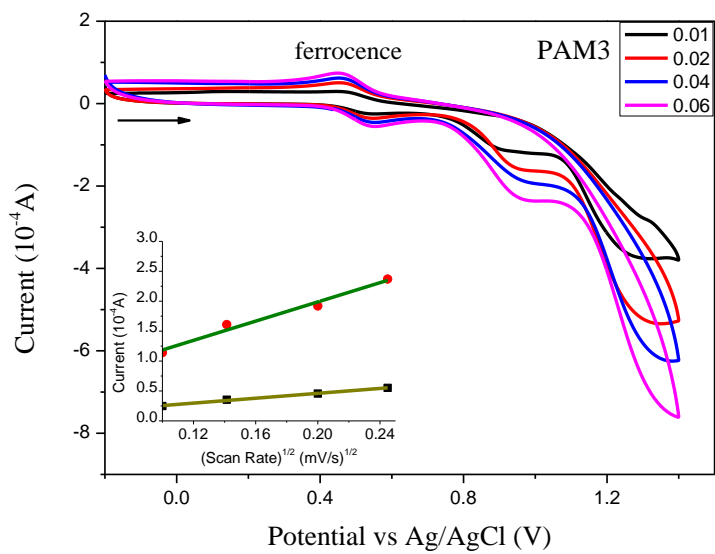
Fig. S7. The differential pulse voltammogram (DPV) of PAM2, PAM3 and PAM5 in CH$_3$CN containing 0.1mol/L LiClO$_4$, at a scan rate of 50 mV/s.
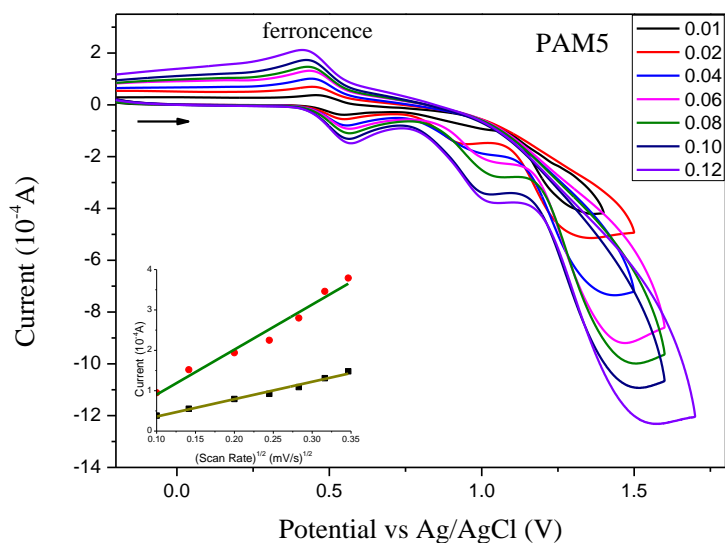
Fig. S8. CVs of PAM3 and PAM5 measured at scan rates between 10 and 120 mV/s. Inset: Randles–Sevcik plot of the oxidation (⬤) peaks of PAM3 and PAM5 relative to ferrocene (◼) measured in dichloromethane with 0.5 M Bu₄ClO₄N as supporting electrolyte. Inset: Relationship of anodic current peaks as a function of the square root scan rate.
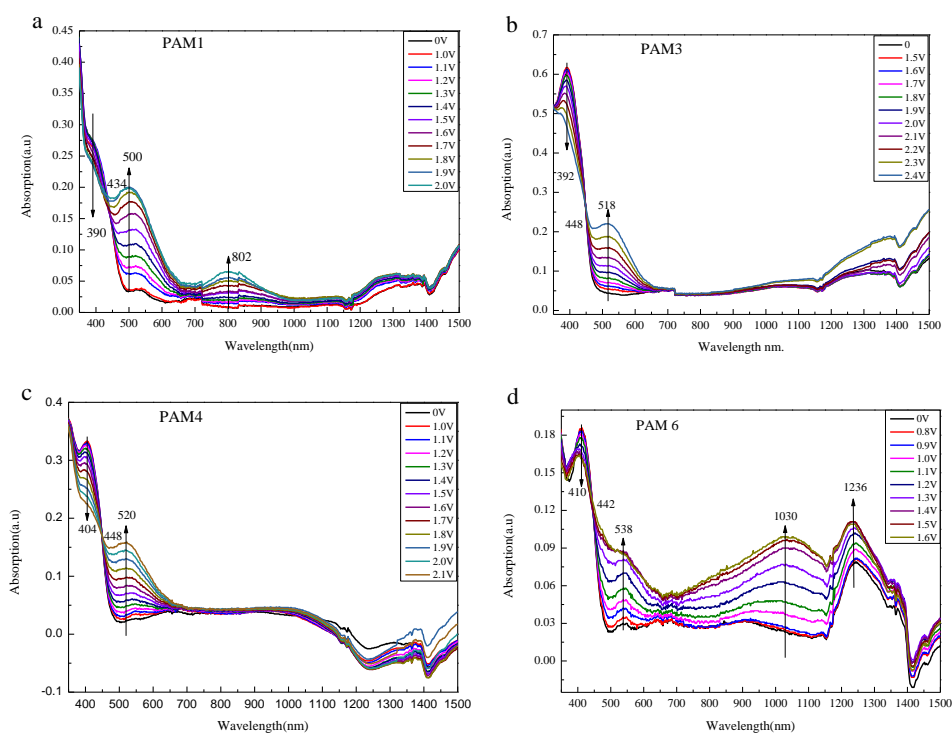

Fig. S9. Electronic absorption spectra of film of PAM1, PAM3, PAM4 and PAM6 membrane respectively, in the process of electrochemical doped with 0.1 V potential intervals in CH_3CN containing 0.1mol/L $LiClO_4$ as the supporting electrolyte (vs Ag/AgCl).